

Real-time renormalization group and charge fluctuations in quantum dots

Herbert Schoeller^{1,2} and Jürgen König³

¹*Forschungszentrum Karlsruhe, Institut für Nanotechnologie, 76021 Karlsruhe, Germany*

²*Institut für Theoretische Festkörperphysik, Universität Karlsruhe, 76128 Karlsruhe, Germany*

³*Department of Physics, Indiana University, Bloomington, Indiana 47405, USA*

(September 15, 2018)

We develop a perturbative renormalization-group method in real time to describe nonequilibrium properties of discrete quantum systems coupled linearly to an environment. We include energy broadening and dissipation and develop a cutoff-independent formalism. We present quantitatively reliable results for the linear and nonlinear conductance in the mixed-valence and empty-orbital regime of the nonequilibrium Anderson impurity model with finite on-site Coulomb repulsion.

72.10.Bg, 73.23.Hk, 05.10.Cc, 05.60.Gg

Renormalization group (RG) methods are standard tools to describe various aspects of condensed-matter problems beyond perturbation theory [1]. Many impurity problems have been treated by numerical RG with excellent results both for thermodynamic quantities and spectral densities [2,3]. These RG techniques, however, cannot describe nonequilibrium properties like the nonlinear conductance, the nonequilibrium stationary state, or the full time development of an initially out-of-equilibrium system. To address these aspects we present here a perturbative RG method, formulated for strongly-correlated quantum systems with a finite number of states coupled linearly to external heat or particle reservoirs. Fundamentally new, we work on a Keldysh contour and generate non-Hamiltonian dynamics during RG, which captures the physics of finite life times and dissipation. Furthermore, no initial or final cutoff in energy or time space is needed, i.e., large and small energy scales are accounted for correctly like in flow-equation methods [4]. Although correlation functions can also be studied, physical quantities like spin and charge susceptibilities or the current can be calculated directly without the need of nonequilibrium Green's functions.

The purpose of our RG technique is to describe quantum fluctuations which are induced by strong coupling between a small quantum system and an environment. There are several recent experiments which show the importance of quantum fluctuations in metallic single-electron transistors [5] and semiconductor quantum dots [6–8] (see [9] for an overview over theoretical papers). Due to the renormalization of resistance and local energy excitations, anomalous line shapes of the conductance have been observed, which can not be explained by golden-rule theories. Therefore, the RG approach presented here can treat simultaneously strong coupling to the reservoirs, strong Coulomb interaction on the island, and finite bias voltage. We apply the technique to a quantum dot with one spin-degenerate state and present for the first time quantitatively reliable results for the nonlinear conductance in the mixed-valence and empty-orbital regime. For applications to the single-electron box

and the single-electron transistor we refer to Ref. [10].

We consider the nonequilibrium Anderson impurity model with finite on-site Coulomb repulsion U . It consists of a single, spin-degenerate state in a quantum dot which is coupled via tunneling to a left and right reservoir. The Hamiltonian $H = H_{res} + H_D + H_T$ consists of three parts. $H_{res} = \sum_{k\sigma r} \epsilon_{k\sigma r} a_{k\sigma r}^\dagger a_{k\sigma r}$ describes two reservoirs, $r = L, R$, where k labels the states and σ denotes the spin. The isolated quantum dot is given by $H_D = \sum_{\sigma} \epsilon_{\sigma} n_{\sigma} + U n_{\uparrow} n_{\downarrow}$ with $n_{\sigma} = c_{\sigma}^\dagger c_{\sigma}$. The coupling to the reservoirs is described by the standard tunneling Hamiltonian $H_T = \sum_{k\sigma r} (T_k^r a_{k\sigma r}^\dagger c_{\sigma} + h.c.)$. The goal is to evaluate the reduced density matrix of the dot system, $\rho_D(t) = \text{Tr}_{res} \rho(t)$, and the expectation value of the current operator $I = I_L = ie \sum_{k\sigma} (T_k^L a_{k\sigma L}^\dagger c_{\sigma} - h.c.)$.

We start with the time evolution of the dot system, $\rho_D(t) = \text{Tr}_{res} \{e^{-iHt} \rho(0) e^{iHt}\}$. Initially, the system is decoupled, and each reservoir is in thermal equilibrium, $\rho(0) = \rho_D(0) \rho_L^{eq} \rho_R^{eq}$. Nonequilibrium situations arise when the two reservoirs have different electrochemical potentials μ_r . As in Refs. [9,11] we expand the forward/backward propagators $\exp(\mp iHt)$ in H_T , and perform the trace Tr_{res} by applying Wick's theorem with respect to the reservoir field operators. All terms can be represented diagrammatically as shown in Fig. 1. Tunneling vertices are ordered along a closed Keldysh contour. They are connected in pairs by the contractions (dashed lines in Fig. 1) $\gamma_r^+(t) = \sum_k |T_k^r|^2 \langle a_{k\sigma r}^\dagger(t) a_{k\sigma r} \rangle$ or $\gamma_r^-(t) = \sum_k |T_k^r|^2 \langle a_{k\sigma r}(t) a_{k\sigma r}^\dagger \rangle$, depending on the relative time-ordering of the vertices on the contour. We obtain for $r = L, R$,

$$\gamma_r^\pm(t) = \frac{-i\Gamma_r e^{\pm i\mu_r t}}{2\beta \sinh[\pi(t - i0^+)/\beta]} \quad (1)$$

with $\beta = 1/(k_B T)$, and $\Gamma_r = 2\pi \sum_k |T_k^r|^2 \delta(E - \epsilon_{k\sigma r})$. The solid line in Fig. 1 represents free time evolution of the dot. As a result, we have obtained an effective theory of the dot degrees of freedom while the reservoirs have been integrated out.

To derive a kinetic equation we will call diagrams irreducible if any vertical cut crosses at least one dashed

line. Fig. 1 shows four such irreducible blocks (a)-(d). We denote the sum over all irreducible diagrams between t' and t by the kernel $\Sigma(t - t')$. The full time evolution, i.e., a sequences of Σ blocks, can be described by a self-consistent equation. Differentiating with respect to time t leads to the standard kinetic equation [9,11]

$$\dot{\rho}_D(t) + iL_D \rho_D(t) = \int_0^t dt' \Sigma(t - t') \rho_D(t'). \quad (2)$$

Here, $L_D = [H_D, \cdot]$ and Σ are superoperators acting on $\rho_D(t)$, i.e., the $4^4 = 256$ matrix elements $\Sigma_{s_1 s'_1, s_2 s'_2}$ are labeled by four dot-states with $s_{1/2}$ ($s'_{1/2}$) referring to the forward (backward) propagator. The l.h.s of Eq. (2) describes the time evolution of the dot in the absence of tunneling whereas the r.h.s contains the dissipative part which drives the dot distribution into a stationary state. In Laplace space Eq. (2) reads $[z - L_D - i\tilde{\Sigma}(z)]\tilde{\rho}_D(z) = i\rho_D(0)$. Thus, the knowledge of $\tilde{\Sigma}(z)$ provides the full time evolution of the dot distribution. The stationary solution follows from $[L_D + i\tilde{\Sigma}(0)]\rho_D^{st} = 0$. The different electrochemical potentials of the reservoirs (leading to a nonequilibrium stationary state) enter via the pair contractions (1) in the kernel $\tilde{\Sigma}(z)$.

Sequential tunneling or the *golden rule* results [12] can be recovered by calculating the kernel $\tilde{\Sigma}(z)$ perturbatively in first order in the tunneling coupling Γ_r . The aim of the present paper, however, is to go beyond and calculate the kernel nonperturbatively by a systematic RG procedure. The idea is to integrate out all contraction lines one after another, beginning with the shortest one. Fig. 1 shows four examples (a)-(d) in second order in Γ . In these examples, the lines with index R are integrated out first. This leads to a renormalization of the dot propagator in (a) and the tunneling vertex in (c). In (b) and (d) the contraction line R connects the forward with the backward propagator. This element does not occur in any equilibrium theory but arises for a Keldysh contour in a natural way. Such contractions lead to non-Hamiltonian dynamics for the dot distribution and, therefore, account for dissipation. To treat these cases in the same way as (a) and (c), it is convenient to view the forward and backward propagator formally as one double line, see Fig. 2. As a consequence, (b) and (d) fall into the same topological classes as (a) and (c), respectively. The price is that a "state" on the double line has to be specified by two dot states, one for the upper and one for the lower propagator. This leads to the superoperator matrix notation used in Eq. (2). The tunneling vertices C_μ^p on the double line act on these double states. There are 16 different vertices, specified by four indices, p and $\mu \equiv \eta\sigma r$, where $p = \pm$ indicates whether the unrenormalized vertex acts on the forward/backward propagator, $\eta = \pm$ represents tunneling in/out, $\sigma = \uparrow, \downarrow$ is the spin, and $r = L, R$ refers to the reservoir index. As shown in example (d) of Fig. 1, after being renormalized a vertex will in general act on

both the forward and backward propagator simultaneously. Double lines without vertices corresponds to a free time evolution $\exp(-iL_D t)$ of the dot (with renormalized L_D). Finally, we denote the rightmost (leftmost) vertex of the kernel $\tilde{\Sigma}$ by A_μ^p (B_μ^p). They are renormalized in a different way than C_μ^p .

The flow parameter t_c in our RG procedure is the largest length of those contractions that have already been integrated out. An infinitesimal RG step is established by integrating out all contractions with a length t between t_c and $t_c + dt_c$. For $t_c \rightarrow \infty$ all contractions are integrated out. We find the RG equations (summation over repeated indices implicitly assumed)

$$\frac{d\tilde{\Sigma}}{dt_c} = -\gamma_{\mu\mu'}^{pp'}(t_c) I_{pp'} A_\mu^p(t_c) B_{\mu'}^{p'}, \quad (3)$$

$$\frac{dL_D}{dt_c} = -i\gamma_{\mu\mu'}^{pp'}(t_c) I_{pp'} C_\mu^p(t_c) C_{\mu'}^{p'}, \quad (4)$$

$$\begin{aligned} \frac{dC_\mu^p}{dt_c} = & \gamma_{\mu_1\mu'_1}^{p_1p'_1}(t_c) \int_0^{t_c} dt [pp'_1 I_{p_1p'_1} C_{\mu_1}^{p_1}(t) C_{\mu'}^{p'} \\ & - C_\mu^p I_{p_1p'_1} C_{\mu_1}^{p_1}(t)] C_{\mu'_1}^{p'_1}(t - t_c), \end{aligned} \quad (5)$$

$$\begin{aligned} \frac{dA_\mu^p}{dt_c} = & \gamma_{\mu_1\mu'_1}^{p_1p'_1}(t_c) \int_0^{t_c} dt [pp'_1 I_{p_1p'_1} A_{\mu_1}^{p_1}(t) C_{\mu'}^{p'} \\ & - A_\mu^p I_{p_1p'_1} C_{\mu_1}^{p_1}(t)] C_{\mu'_1}^{p'_1}(t - t_c), \end{aligned} \quad (6)$$

$$\begin{aligned} \frac{dB_\mu^p}{dt_c} = & \gamma_{\mu_1\mu'_1}^{p_1p'_1}(t_c) \int_0^{t_c} dt \\ & pp'_1 I_{p_1p'_1} C_{\mu_1}^{p_1}(t) C_\mu^p B_{\mu'_1}^{p'_1}(t - t_c), \end{aligned} \quad (7)$$

We introduced $\gamma_{\mu\mu'}^{pp'}(t) = \gamma_r^{-p'\eta}(p't)\delta_{\bar{\mu}\mu'}$ for the contraction between two tunneling vertices on the double line ($\mu \equiv \eta\sigma r$, $\bar{\mu} \equiv -\eta\sigma r$, $\mu' \equiv \eta'\sigma'r'$) to get a compact notation. The interaction picture is defined by $C_\mu^p(t) = e^{iL_D t} C_\mu^p e^{-iL_D t}$, $A_\mu^p(t) = e^{izt} A_\mu^p e^{-iL_D t}$, and $B_\mu^p(t) = e^{iL_D t} B_\mu^p e^{-izt}$. The diagonal superoperator $I_{pp'}$ together with the factors pp'_1 account for possible minus signs due to Fermi statistics. We get $(I_{pp'})_{ss',ss'} = (pp')^{N_s - N_{s'}}$, where N_s is the particle number for state s . All terms arise naturally from our intuitive picture set up in Fig. 2 except for the second term on the r.h.s of Eqs. (5) and (6). The latter are correction terms to account for correct time ordering [13].

To evaluate the average current we repeat the above derivation of the RG equations but replace the unrenormalized boundary vertex operator A_μ^p by the current vertex I . The analog of Eq. (3) gives the current kernel $\tilde{\Sigma}_I(z)$ and the current follows from $\langle I \rangle(z) = \text{Tr}_D \tilde{\Sigma}_I(z) \tilde{\rho}(z)$.

Taking matrix elements, all integrals in Eqs. (5)-(7) can be calculated analytically, and pure differential equations are left which we solve numerically. Most of the matrix elements which are initially zero remain unchanged under the RG flow. We end up with 26 equations for $\tilde{\Sigma}$

and L_D each, and 192 equations for C , A , and B each to solve.

The RG flow of conventional poor man scaling and operator product expansion methods stops at some "characteristic" time (or inverse energy) scale. All results, therefore, depend on a low-energy cutoff. This is *not* the case in our formulation since we have *not* expanded the propagation $\exp(\pm iL_D t_c)$ in t_c (it occurs in the interaction picture of the vertex operators) and can, therefore, integrate out *all* time scales. Furthermore, we work on a Keldysh contour and find that the renormalized L_D -operator of the dot system can no longer be represented as the commutator with a renormalized Hamiltonian $L_D \neq [H_D, \cdot]$. This corresponds to non-Hamiltonian dynamics and is needed to describe the physics of dissipation and finite life times.

An important question concerns the validity range of the present approach. Although no general statement is possible, the RG flow itself will indicate the breakdown of the procedure by instabilities or increasing coupling constants. Due to the neglect of higher-order vertex corrections, one might not trust the procedure for too large coupling constants. However, for the specific example of the Anderson model in the mixed-valence regime (see below) we reproduce exact Bethe ansatz solutions within high accuracy even in the strong-coupling regime. The same was achieved for the ground-state energy of the single-electron box [10]. A possible explanation is the generation of rates and energy broadening during RG which improves the accuracy and sets another energy scale for the cutoff of the RG flow (for the present problem given by Γ). This is consistent with our numerical solution and with a recent analysis of poor man scaling on a Keldysh contour in Ref. [14].

In Fig. 3 we show the linear conductance G for the Anderson model as function of $\epsilon = \epsilon_\sigma$, which is varied experimentally by the gate voltage. For $T = 0$ and $\epsilon > -0.4\Gamma$, the deviation from the exact Friedel sum rule $G|_{T=0} = (2e^2/h) \sin^2(\pi\langle n \rangle/2)$ is less than 2%. Here, $\Gamma/2 = \Gamma_L = \Gamma_R$ and $\langle n \rangle = \sum_\sigma \langle n_\sigma \rangle$. In the same regime, the average occupation $\langle n \rangle$ agrees with the exact Bethe ansatz solution [15] within 3% (inset of Fig. 3). Since the RG flow is strongest if both temperature and bias voltage vanish, this comparison gives good support that our results are reliable in the whole mixed-valence and empty-orbital regime for all temperatures and bias voltages. Furthermore, we find excellent agreement with the exact Bethe ansatz solution for the magnetic and charge susceptibility at $\epsilon = 0$ as function of T and U , respectively [16]. Thus, the neglect of higher-order vertex terms seems to be justified.

In the Kondo regime, i.e., for $\epsilon \lesssim -0.4\Gamma$, spin fluctuations are dominant and double-vertex terms become important. In this regime, deviations from the Friedel sum rule can be seen in Fig. 3. Experimentally, such deviations occur as well [6–8], since it is difficult to reach

the $T = 0$ limit. Our theory accounts for charge fluctuations very well which are responsible for the temperature-dependent renormalization of the dot level as shown by the shift of the maximum peak in Fig. 3. The fact that the conductance increases along the zero temperature result on the r.h.s of the conductance peak is in good agreement with experiments [6,7]. A fit of the temperature dependence of the linear conductance to the experiment in Ref. [6] is shown in Fig. 4 for various values of ϵ . The agreement is quite well except for $T \gtrsim 0.5\Gamma$ where the experimental conductance is higher. A reason for this discrepancy might be the presence of other levels with a level spacing of order Γ . For a low-lying level the conductance increases monotonically with decreasing temperature and finally saturates. The saturated value at $T = 0$ is not identical to the unitary limit $(e^2/h)8\Gamma_L\Gamma_R/\Gamma^2$ since we are still in the mixed-valence regime. However, the value agrees perfectly with the Friedel sum rule as already stated above. In the empty-orbital regime, $\epsilon \gtrsim 0$, the conductance shows a local maximum by varying T . Here, the renormalized ϵ is above the Fermi level and will be occupied at high enough temperature. This increases the conductance with increasing T .

Fig. 5 shows $G = dI/dV$ as a function of the bias voltage for $\epsilon = -0.4\Gamma$. We obtain a zero-bias maximum with an amplitude increasing monotonically with decreasing T (see Fig. 4). This maximum is *not* due to the presence of a Kondo resonance but stems from the renormalized dot level being near the Fermi levels of the reservoirs. The width of the peak in Fig. 5 scales with Γ which is the relevant energy scale in the mixed-valence regime. Since the zero-bias maximum has a symmetric line shape, our results can be used for a fit of the important energy scale Γ in experiments.

In summary we have presented a new RG technique to calculate nonequilibrium properties of dissipative quantum systems beyond perturbation theory. The method is very flexible and was applied to the Anderson-impurity model with finite U . In the mixed-valence and empty-orbital regime the Friedel sum rule and the exact Bethe ansatz solution were reproduced at zero temperature. The results are consistent with experiments.

We acknowledge useful discussions with T. Costi, J.v. Delft, D. Goldhaber-Gordon, H. Grabert, M. Hettler, G. Schön, K. Schönhammer, and P. Wölffe. We thank U. Gerland for providing us with the Bethe ansatz results, and D. Goldhaber-Gordon for the experimental data. This work was supported by the Swiss National Science Foundation (H.S.) and by the "Deutsche Forschungsgemeinschaft" as part of "SFB 195".

- [1] P.W. Anderson, J. Phys. C **3**, 2346 (1970); K.G. Wilson, Rev. Mod. Phys. **47**, 773 (1975).
- [2] H.R. Krishna-murthy, J.W. Wilkins, and K.G. Wilson, Phys. Rev. B **21**, 1003 (1980); Phys. Rev. B **21**, 1043 (1980).
- [3] T.A. Costi, A.C. Hewson, and V. Zlatić, J. Phys. C **6**, 2519 (1994).
- [4] S.D. Glazek and K.G. Wilson, Phys. Rev. D **48**, 5863 (1993); F. Wegner, Ann. Physik (Leipzig), **3**, 77 (1994).
- [5] P. Joyez, V. Bouchiat, D. Esteve, C. Urbina, and M.H. Devoret, Phys. Rev. Lett. **79**, 1349 (1997).
- [6] D. Goldhaber-Gordon *et al.*, Nature (London), **391**, 156 (1998); Phys. Rev. Lett. **81**, 5225 (1998).
- [7] S.M. Cronenwett *et al.*, Science **281**, 540 (1998).
- [8] J. Schmid *et al.*, Physica B **256-258**, 182 (1998); F. Simmel *et al.*, Phys. Rev. Lett. **83**, 804 (1999).
- [9] H. Schoeller, in 'Mesoscopic Electron Transport', eds. L.L. Sohn *et al.* (Kluwer 1997), p. 291-330.
- [10] J. König and H. Schoeller, Phys. Rev. Lett. **81**, 3511 (1998); F. Kuczera, H. Schoeller, J. König, and G. Schön, preprint.
- [11] H. Schoeller and G. Schön, Phys. Rev. B **50**, 18436 (1994); J. König *et al.* Europhys. Lett. **31**, 31 (1995); Phys. Rev. Lett. **76**, 1715 (1996).
- [12] D.V. Averin *et al.* Phys. Rev. B **44**, 6199 (1991); C.W.J. Beenakker, Phys. Rev. B **44**, 1646 (1991).
- [13] Time misordering happens since the contractions in Fig. 1a and 1b renormalizing L_D are two-time objects but L_D is treated after renormalization as a single-time one. For further details of this subtle point and a more detailed derivation of the RG equations we refer to a forthcoming longer paper.
- [14] A. Kaminski, Yu.V. Nazarov, and L.I. Glazman, Phys. Rev. Lett. **83**, 384 (1999).
- [15] A.M. Tsel'ick and P.B. Wiegmann, Adv. in Physics **32**, 453 (1983).
- [16] N. Kawakami and A. Okiji, J. Phys. Soc. Jap. **51**, 2043 (1982); A. Okiji and N. Kawakami, Phys. Rev. Lett. **50**, 1157 (1983).

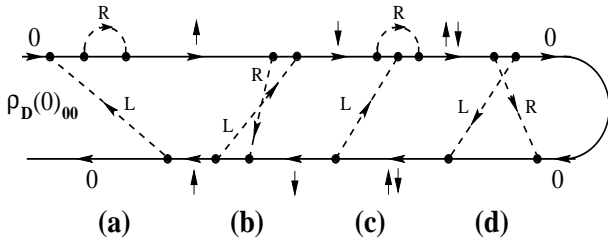


FIG. 1. Example of a diagram on the Keldysh contour for the matrix element $\rho_D(t)_{00}$. The contractions are labeled by the reservoir indices L and R .

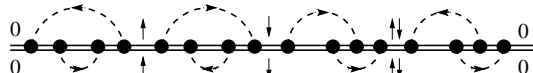


FIG. 2. The same figure as Fig. 1 but the two lines taken together.

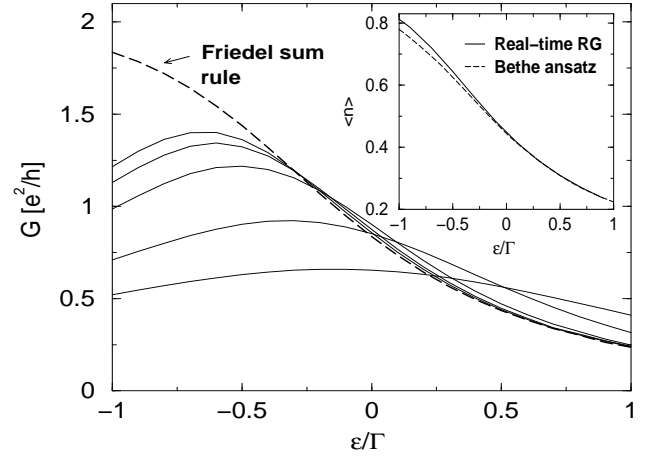


FIG. 3. Linear conductance as a function of the dot level. $T/\Gamma = 0, 0.05, 0.1, 0.25, 0.5$ (solid lines from top to bottom) and $U = 6\Gamma$. The inset shows the average occupation for $T = 0$.

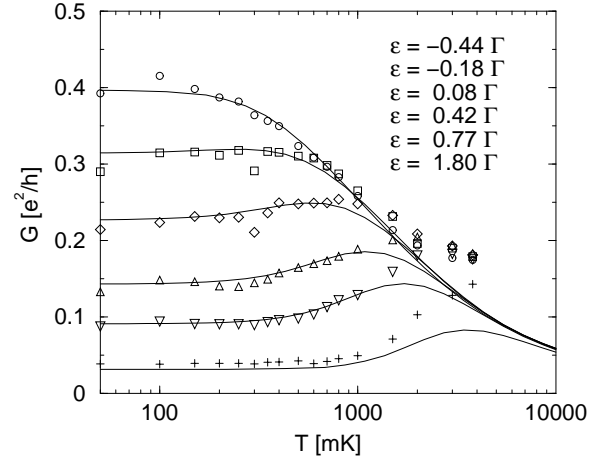


FIG. 4. Linear conductance as a function of temperature in comparison to experiment [6]. $U = 6.2\Gamma$, $8\Gamma_L\Gamma_R/\Gamma^2 = 0.6$, and $\Gamma = 3423\text{mK}$.

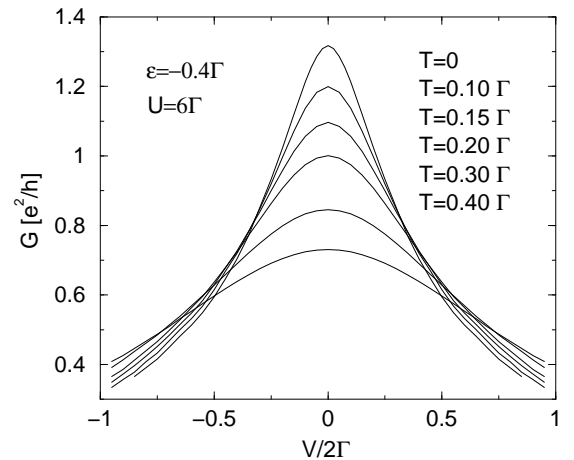


FIG. 5. Nonlinear conductance as a function of the bias voltage.

